PHYSICAL REVIEW B **91**, 235426 (2015)

Multiplet features and magnetic properties of Fe on Cu(111): From single atoms to small clusters

Giulia E. Pacchioni,[1] Luca Gragnaniello,[1] Fabio Donati,[1] Marina Pivetta,[1] Gabriel Autès,[2] Oleg V. Yazyev,[2] Stefano Rusponi,[1] and Harald Brune[1]

[1]*Institute of Condensed Matter Physics, Ecole Polytechnique Fédérale de Lausanne (EPFL), CH-1015 Lausanne, Switzerland*

[2]*Institute of Theoretical Physics, Ecole Polytechnique Fédérale de Lausanne (EPFL), CH-1015 Lausanne, Switzerland*

(Received 12 March 2015; revised manuscript received 20 May 2015; published 16 June 2015)

The observation of sharp atomiclike multiplet features is unexpected for individual 3*d* atoms adsorbed on transition-metal surfaces. However, we show by means of x-ray absorption spectroscopy and x-ray magnetic circular dichroism that individual Fe atoms on Cu(111) exhibit such features. They are reminiscent of a low degree of hybridization, similar to 3*d* atoms adsorbed on alkali-metal surfaces. We determine the spin, orbital, and total magnetic moments, as well as magnetic anisotropy energy for the individual Fe atoms and for small Fe clusters that we form by increasing the coverage. The multiplet features are smoothened and the orbital moment rapidly decreases with increasing cluster size. For Fe monomers, comparison with density functional theory and multiplet calculations reveals a d^7 electronic configuration, owing to the transfer of one electron from the 4*s* to the 3*d* states.

DOI: 10.1103/PhysRevB.91.235426 PACS number(s): 75.30.Gw, 75.75.−c, 78.70.Dm, 71.15.Mb

I. INTRODUCTION

Magnetic transition-metal atoms and clusters adsorbed on nonmagnetic surfaces are model systems to study the effect of reduced coordination of the atoms, which is expected to result in an enhancement of the magnetic orbital moment and anisotropy [1–4]. In particular, Fe adatoms and clusters adsorbed on Cu(111) have been the subject of many studies aiming at the determination of their magnetic properties, both from the theoretical and from the experimental points of view. For example, spin-polarized scanning tunneling microscopy (SP-STM) has been used to assemble Fe atoms on Cu(111) into chains able to perform logical operations [5], or into clusters with different geometries to investigate their magnetic properties on an atom-by-atom basis [6]. In both cases, the Fe atoms had interatomic distances of a few Cu(111) lattice sites. Moreover, five-atom Fe clusters adsorbed on Cu(111) were reported to exhibit magnetic remanence at $T = 0.3$ K with a relaxation time longer than two hours, and were thus demonstrated to be the smallest stable magnet ever constructed [7].

Single atoms adsorbed on metal surfaces normally experience strong hybridization, leading to electron delocalization and loss of the atomic character of the electronic states. In the case of Fe atoms on Cu(111), SP-STM measurements suggest a localized character of the electrons enabling spin excitations, combined with a strong hybridization responsible for the very short observed spin-state lifetime [8]. At the same time, a model treating five-atom Fe clusters as a quantum system with ideal half-integer spin reproduces correctly the experimental results [7]. Fe atoms on alkali-metal surfaces exhibit multiplet structures in photoemission spectra, with the degree of atomiclike behavior depending on the chosen substrate [9]. On the other hand, on the surfaces of 5*d* and 4*d* elements, such as Pt(111) [10,11], Rh(111), and Pd(111) [12], Fe atoms are known to be strongly hybridized. Cu(111) has an *s*-like density of states at the Fermi energy, bringing it close to alkali-metal surfaces, but at the same time is a 3*d* metal, thus it is not trivial to say whether a strong or a weak degree of hybridization is expected. To clarify this question, we studied Fe atoms on Cu(111) with x-ray absorption spectroscopy (XAS) and x-ray magnetic circular dichroism (XMCD).

XAS and XMCD, thanks to their element specificity and their high sensitivity, are powerful tools for the study of magnetic materials. With these techniques it is possible to probe systems with an adatom concentration as low as 0.002 monolayers (ML) [13]. Despite the finite spatial extent of the x-ray beam, making XAS and XMCD spatially averaging techniques, the properties of single atoms can be probed if the system is composed of noninteracting monomers. Thanks to the sum rules [14,15] XMCD allows to separately determine the spin and orbital contributions to the magnetic moment. From angular-dependent XMCD measurements as a function of an applied magnetic field it is also possible to determine the magnetic anisotropy energy (MAE), which is a key parameter for obtaining stable magnetization since its magnitude determines the probability of thermally induced magnetization reversal.

In this work, we use XAS and XMCD to study the magnetic properties of both atoms and small clusters of Fe on Cu(111). For Fe monomers, we report on the unexpected observation of multiplet features and on their disappearance upon increasing coverage. By comparing the experimental data with density functional theory (DFT) and multiplet calculations, we find a d^7 electronic configuration, owing to the transfer of one electron from the 4*s* to the 3*d* states. The MAE of single atoms and the evolution of orbital (μ_L) and spin (μ_S) magnetic moments as a function of coverage are addressed.

II. EXPERIMENT

Experiments were performed at the EPFL/PSI X-Treme beamline [16] at the Swiss Light Source. The end station includes a chamber for the sample preparation equipped with a scanning tunneling microscope (STM), from which samples can be transferred into the cryostat for XAS and XMCD measurements without breaking the vacuum. The Cu(111) crystal was prepared by Ar^+ sputtering (0.8 μA/cm^2, 1200 eV, 20 min) and annealing (800 K, 20 min) cycles in the preparation chamber, and Fe was deposited from an *e*-beam

evaporator on the substrate held at $T_{dep} \approx 3.5$ K directly in the cryostat. We investigated Fe coverages ranging from $\Theta_{Fe} = 0.007$ to 0.145 ML [one monolayer (ML) is defined as one Fe atom per Cu(111) unit cell] in order to have access to both isolated impurities and small clusters. The Fe coverage was calibrated by correlating XAS and STM data, and the deposition rate was set to 0.007 ML/min.

Measurements were taken at the $L_{2,3}$ absorption edges of Fe, resulting from the excitation of $2p$ core electrons into empty $3d$ states. We used circularly polarized x rays, with μ_+ and μ_- referring to parallel, respectively, antiparallel alignment of the helicity with respect to the beam direction. The XAS spectra were recorded in the total electron yield mode and normalized to the intensity of the x-ray beam measured on a metallic grid placed upstream of the sample. XMCD spectra were obtained as the difference between the XAS signal of the two polarizations, and they were normalized to the Fe coverage. Both the out-of-plane and in-plane XAS and XMCD signals were investigated by rotating the sample from $\theta = 0^\circ$ to 60° between sample normal and x-ray beam. Element specific magnetization curves were recorded as the ratio between the amplitude of the L_3 XMCD intensity at the peak and the intensity at the pre-edge, at both normal and grazing incidence. All measurements were performed at $T = 2.5$ K and in magnetic fields up to $B = \pm 6.8$ T parallel to the x-ray beam.

III. RESULTS AND DISCUSSION

A. Fe monomers on Cu(111)

To investigate the magnetic properties of Fe monomers on Cu(111), we prepared a sample with $\Theta_{Fe} = 0.007$ ML. Figure 1 shows XAS and XMCD spectra measured for normal and grazing incidence. Multiplet structures, not observed in bulk spectra [17], can be clearly seen for both angles of incidence. In the XAS, a splitting of the L_2 peak is observed, both for μ_+ and μ_-, and the L_2 peak in the XMCD spectra, found at 716.0 eV, originates from the lower-energy component of the XAS peak. Also on the L_3 peak the μ_- component is split, as shown in the inset, and also in this case the corresponding XMCD peak, measured at 703.2 eV, comes from the lower-energy component of the XAS feature. Moreover, multiple shoulders are present on the sides of the L_3 peak both in the XAS and in the XMCD spectra (see labeled energies), and in the latter a small positive feature at the onset of the L_3 peak is observed.

These features are reminiscent of the spectra measured for Fe atoms on alkali metals [9,13] or thin oxide films [18], suggesting an electronic configuration close to $3d^7$. Our spectra are more atomiclike than the ones reported for Fe/Cu(100) [10,19], as expected from the reduced number of nearest neighbors on Cu(111) with respect to Cu(100), and coherent with the higher orbital magnetic moment predicted by DFT for Fe/Cu(111) ($\mu_L = 0.65\mu_B$) with respect to Fe/Cu(100) ($\mu_L = 0.47\mu_B$) [20].

To determine the electronic configuration of the Fe atoms, we performed multiplet calculations[1] using the CTM4XAS55

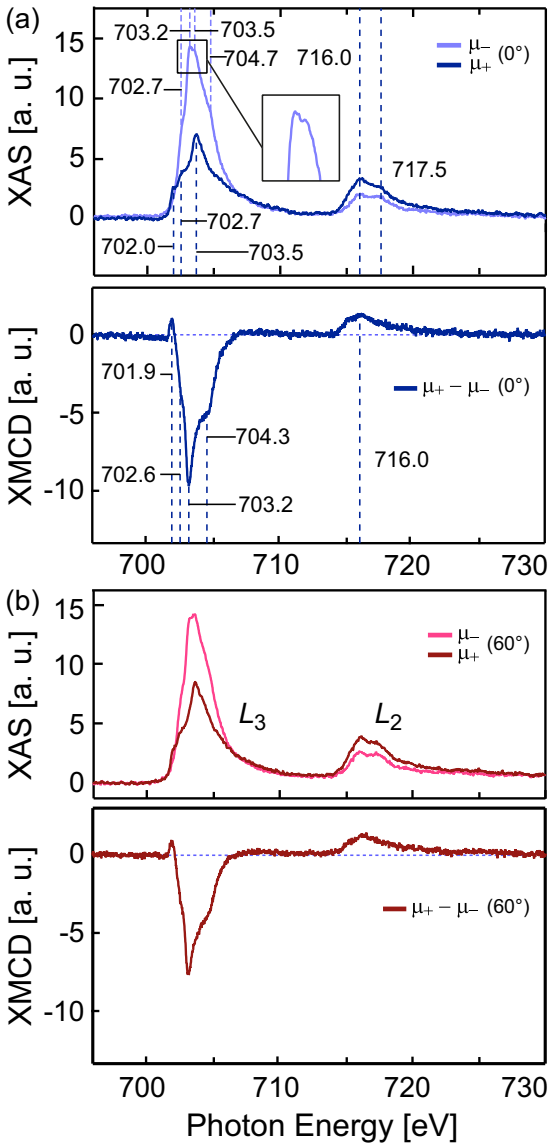

FIG. 1. (Color online) Background subtracted XAS and XMCD spectra for Fe monomers on Cu(111), measured at the Fe $L_{2,3}$ absorption edges at $T = 2.5$ K and with $B = 6.8$ T collinear with the x-ray beam. Spectra are taken with parallel (μ_+) and antiparallel (μ_-) alignment of light helicity with respect to B. (a) Normal incidence; (b) grazing incidence. XMCD spectra have been normalized to the Fe coverage determined by the integral of the $\mu_+ + \mu_-$ spectrum over the $L_{2,3}$ edges. The L_3 peak of the μ_- component of XAS is magnified in the inset. $\Theta_{Fe} = 0.007$ ML.

[1]Configuration interaction is allowed respecting the $C_{\infty,v}$ symmetry, therefore, we used the hopping integrals $t(a_1) = 0.3$ eV, $t(e_1) = 1.0$ eV, and $t(e_2) = 1.0$ eV. The charge transfer energy Δ and the core-hole interaction $U_{p-d} - U_{d-d}$ were set to -10.0 and 1.0 eV, respectively. Default values for the Slater-Condon integrals have been used, corresponding to a reduction to 80% of the Hartree-Fock values. Transition amplitudes for L_2 and L_3 were calculated in a dipolar approximation and broadened with Lorentzian functions of FWHM = 0.45 and 0.15 eV, respectively, to reproduce the experimental spectra. Further Gaussian broadening of 0.35 eV was introduced to include the finite experimental energy resolution.

code [21]. To a first approximation, a $C_{\infty,v}$ symmetry was assumed for the crystal field experienced by the atom. This symmetry is generated by the sea of s-like conduction electrons of the Cu substrate, creating a vertically homogeneous electrostatic repulsion, while the d states, being well below E_F, do not contribute. This uniaxial crystal field lifts the degeneracy of the d orbitals producing an a_1 singlet (d_{z^2}) and two doublets e_1 (d_{xz},d_{yz}) and e_2 ($d_{x^2-y^2}$,d_{xy}). Best fits obtained by optimizing the multiplet calculation parameters to describe the XAS and XMCD spectra measured at normal incidence are shown in Fig. 2. The deviation of the calculated curves from the experimental ones on the high-energy shoulders of the L_2 and L_3 peaks can be attributed to the fact that multiplet calculations can not correctly take into account the whole hybridization with the surface [19]. We find that the ground state is well described by a mixed electronic configuration consisting of 3% $3d^6$ and 97% $3d^7$, corresponding to a number of holes $h_d = 3.03$. We note that even a weak configuration interaction can make an important difference in the resulting spectra, as it may cause splitting of degenerate levels and/or additional state mixing [4]. The calculated splitting of the $3d$ orbitals is shown in the inset of Fig. 2: the e_2 doublet is lowest in energy, followed by the e_1 doublet (135 meV) and finally by the a_1 singlet (180 meV).

Using the number of holes found in the multiplet calculations, orbital and spin magnetic moments can be obtained from the measured spectra using the sum rules [14,15]

$$\mu_L = -\frac{4}{3} h_d \frac{\int_{L_3+L_2}(\mu_+ - \mu_-)dE}{\int_{L_3+L_2}(\mu_+ + \mu_-)dE}, \tag{1}$$

$$\mu_{S+7T} = -h_d \frac{6\int_{L_3}(\mu_+ - \mu_-)dE - 4\int_{L_3+L_2}(\mu_+ - \mu_-)dE}{\int_{L_3+L_2}(\mu_+ + \mu_-)dE}. \tag{2}$$

We obtain $\mu_L = 0.66 \pm 0.04\,\mu_B$ and $\mu_{S+7T} = 2.2 \pm 0.1\,\mu_B$ at normal incidence, and $\mu_L = 0.42 \pm 0.04\,\mu_B$ and $\mu_{S+7T} = 1.80 \pm 0.04\,\mu_B$ at grazing incidence. At normal incidence, the ratio μ_L/μ_{S+7D} is 0.30, more than twice the value of 0.12 obtained for Fe/Pd(111), and twice the one of Fe/Rh(111) (0.15) [12], confirming the reduced hybridization of the present system. The sum rule gives the spin moment together with the spin dipole moment. Experimentally, it is not possible to determine the two contributions individually, however, multiplet calculations give $\mu_{7T} = -0.2\mu_B$ for normal incidence. For grazing incidence, the value of the dipole moment cannot be determined, as saturation is not reached [22]. We note that the L_2 and L_3 edges are not completely separated, which leads to an underestimation of the spin moment of ≈10% [17,23]. Thus, taking into account these values, we can estimate for normal incidence $\mu_S = 2.6 \pm 0.2\mu_B$.

The higher intensity of the L_3 XMCD peak measured at normal incidence with respect to the one measured at grazing incidence implies an out-of-plane easy axis. This is confirmed by the fact that the magnetization curve, shown in Fig. 3, is steeper for $\theta = 0°$ than for $\theta = 60°$ around 0 T. Since the system has a behavior in-between a classical and a quantum one, we used two different approaches to simulate the magnetization curves in order to obtain the average MAE per atom K and the total magnetic moment μ. In a semiclassical model, the magnetization curve can be fit using the

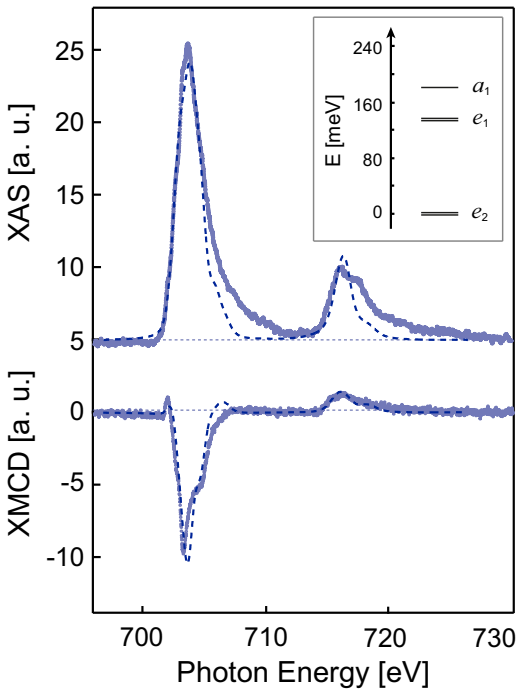

FIG. 2. (Color online) Simulated normal incidence XAS and XMCD spectra (dashed lines) compared with experimental ones for individual Fe atoms on Cu(111) ($\Theta_{Fe} = 0.007$ ML in experiment). Inset: energy splitting of the singlet and doublet states resulting from the $3d$ orbitals as given by the multiplet calculations. XAS and XMCD spectra were best reproduced using a mixed 3% $3d^6$ and 97% $3d^7$ configuration with crystal field terms $10Dq = 0.0$ eV, $Ds = -0.045$ eV, and $Dt = 0.00$ eV.

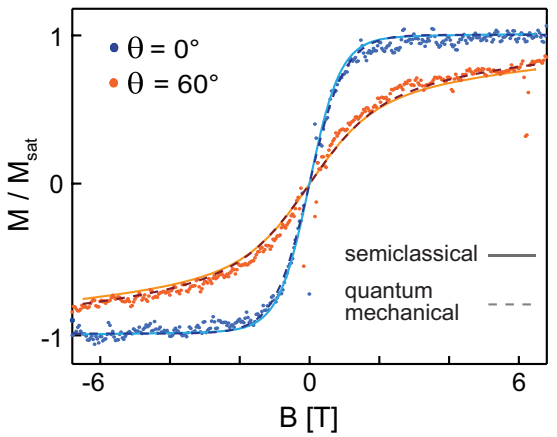

FIG. 3. (Color online) Magnetization curves for normal (blue) and grazing (orange) incidence. The dots represent the amplitude of the L_3 XMDC peak at 703.2 eV divided by the pre-edge intensity at 701.2 eV. The curve measured at grazing incidence is multiplied by the ratio $(\mu_L + \mu_{S+7T})_{grazing}/(\mu_L + \mu_{S+7T})_{normal}$. Solid (dashed) lines represent the fit obtained with the semiclassical (quantum mechanical) model ($\Theta_{Fe} = 0.011$ ML).

formula [1]

$$M = M_{\text{sat}} \frac{\int_0^{2\pi} d\phi \int_0^{\pi} d\theta \, \sin\theta \cos\theta e^{-E(\theta_0,\theta,\phi)/k_B T}}{\int_0^{2\pi} d\phi \int_0^{\pi} d\theta \, \sin\theta e^{-E(\theta_0,\theta,\phi)/k_B T}}, \quad (3)$$

where

$$E(\theta_0,\theta,\phi) = -\mu B \cos\theta - K(\sin\theta_0 \sin\theta \cos\phi + \cos\theta_0 \cos\theta)^2 \quad (4)$$

with θ_0 the easy magnetization direction and **B** taken as z axis.

We find a MAE per atom of $K = 1.8 \pm 0.4$ meV and a total magnetic moment per atom of $\mu = 4.5 \pm 0.5 \mu_B$, where $\mu = \mu_L + \mu_S + \mu_{\text{ind}}$ (Cu) includes the magnetic moment induced on the Cu sites per Fe atom. The calculated curves are shown in Fig. 3 and agree very well with experiment.

In a quantum mechanical approach, we can describe the spin states of an Fe atom using the following spin Hamiltonian:

$$\hat{H}_{\text{spin}} = g\mu_B \hat{\mathbf{S}} \cdot \mathbf{B} + D\hat{S}_z^2, \quad (5)$$

where g is the electron Landé factor, **B** the external magnetic field, D the uniaxial anisotropy parameter, and $\hat{\mathbf{S}}$ the effective spin operator. The z axis is by convention chosen such as to maximize $|D|$. Following the electronic configuration suggested by the multiplet calculations, we modeled our system with an effective spin $S = \frac{3}{2}$, implying half-integer ground- and first-excited-state doublets. The expectation values of the magnetization along the beam axis as a function of **B** are obtained by

$$\langle M_{\theta_0} \rangle = g \langle S_{\theta_0} \rangle = g \frac{\sum_{i=1}^{2S+1} \langle \phi_i | S_{\theta_0} | \phi_i \rangle e^{\epsilon_i / k_B T}}{\sum_{i=1}^{2S+1} e^{\epsilon_i / k_B T}}, \quad (6)$$

where $S_{\theta_0} = \sin\theta_0 S_x + \sin\theta_0 S_y + \cos\theta_0 S_z$ is the spin operator for an arbitrary incidence angle θ_0, while ϕ_i and ϵ_i are the eigenstates and the eigenvalues obtained after diagonalizing the spin Hamiltonian. The parameters g and D were adjusted to fit the experimental data. The obtained curves for both incidence angles are shown as dashed lines in Fig. 3. They almost coincide with the classical curves and agree very well with experiment. We find $g = 2.45 \pm 0.3$ and $D = -0.85 \pm 0.2$ meV, so, having assumed a spin $S = \frac{3}{2}$, we obtain a total magnetic moment $\mu = g\mu_B S = 3.7 \pm 0.5 \mu_B$ and a magnetic anisotropy $K = -2D = 1.7 \pm 0.4$ meV. The values for K in the two models agree within the error bars, while the total moment in the quantum mechanical description is lower than in the semiclassical one, as it was already reported for other systems [24]. The total moment found with the sum rules is $\mu = 3.3 \pm 0.2 \mu_B$, which is compatible with the value obtained with the quantum mechanical model and hints towards a small moment induced on copper atoms. The values for the magnetic moments and for the MAE obtained with the sum rules and with the semiclassical and quantum mechanical models are summarized in Table I. The total moment we find with the sum rules and with the fitting of the magnetization curves is close to $\mu = 3.5 \mu_B$ reported for Fe monomers on Cu(111) by Khajetoorians *et al.* [8]. In the same work, they also find an anisotropy energy K comprised between 0.8 and 1.5 meV. The higher value obtained in our measurements can be understood in the context of a recent publication showing that a lower MAE is expected in dynamical spin excitation measurements compared to static ones [25]. The experimental values for K are not surprising since also on other substrates, such as Ag(111) [26], Pt(111) [10,11], Pd(111), and Rh(111) [12], Fe atoms show an out-of-plane anisotropy and a small value for the MAE, of the order of at most 2 meV, and thereby much smaller than the one measured for Co on Pt(111) [1].

TABLE I. Spin, orbital, and total magnetic moments and the MAE as obtained from the sum rules and from the fit of the magnetization curves with the quantum mechanical (QM) and the semiclassical (SC) models. The corrections to μ_S described in the text are included.

	μ_S (μ_B)	μ_L (μ_B)	μ (μ_B)	K (meV)
Sum rules	2.6 ± 0.2	0.66 ± 0.04	3.3 ± 0.2	
QM model			3.7 ± 0.5	1.7 ± 0.4
SC model			4.5 ± 0.5	1.8 ± 0.4

Multiplet calculations offer a good description of atomic systems with localized electrons. Since our system involves delocalized electrons, we can not blindly rely on them. In order to address the electronic and magnetic properties with a complementary theoretical method, we performed nonrelativistic DFT calculations of a single Fe atom located on a five-layer thick slab of Cu(111) within a (4×4) supercell (see inset in Fig. 4). We used the generalized gradient approximation with a mean-field Hubbard correction (GGA $+U$) [27], as implemented in QUANTUM ESPRESSO [28]. Using the linear-response approach, we estimated the value of the Hubbard U to be 2.9 eV [29]. We verified that different values of U, namely $U = 2.2$ and 4 eV, give very similar results. To find the adsorption position of the Fe adatom, we fully relaxed the structure starting from the four high-symmetry positions (hcp and fcc hollows, top, and bridge). The lowest-energy configuration corresponds to the Fe atom located in the fcc adsorption site at a distance of 1.96 Å above the topmost atomic plane of Cu. The hcp site configuration has a slightly higher energy (by 10 meV) while the bridge and top sites are 0.28 and 0.78 eV higher in energy than the fcc adsorption site, respectively. Preferential adsorption on the fcc site is not surprising, as it has been already reported for this system

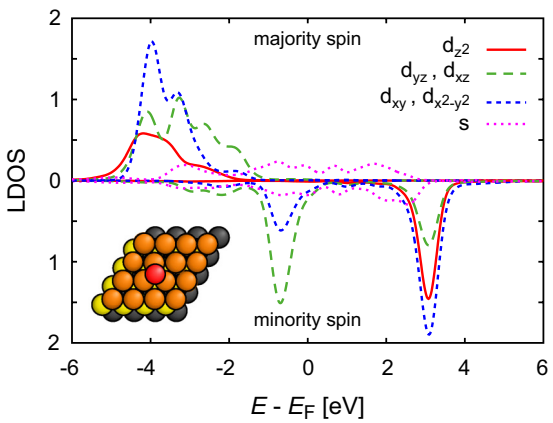

FIG. 4. (Color online) Spin-resolved local density of states projected on the Fe atomic orbitals. The inset shows the geometry of the slab used in DFT calculations.

TABLE II. Löwdin populations and spin polarization of the Fe orbitals from the nonrelativistic DFT calculations.

	Total	4*s* orbitals	3*d* orbitals
Total charge	7.89	1.04	6.85
Spin up	5.57	0.60	4.97
Spin down	2.33	0.44	1.88
Polarization	3.24	0.16	3.09

[8,30]. A similarly small difference of 6 meV in favor of fcc with respect to hcp sites has been reported also for Cu adatoms on Cu(111) [31]. The atomic spin and the electronic configuration of the Fe adatom were obtained by projecting the wave functions of the entire system onto the Fe atomic orbitals. The Löwdin population and the spin polarization of the 4*s* and 3*d* atomic orbitals of Fe are reported in Table II, while the corresponding spin-resolved local density of states plots are shown in Fig. 4.

Our results show that the Fe adatom is close to a $4s^1 3d^7$ configuration, corresponding to $h_d = 3.15$. This value is in good agreement with the one deduced from the multiplet calculations. Fe acts as a donor of ≈ 0.1 e^- transferred to Cu. The spin polarization of the 3*d* states (3.09 μ_B) shows that the Fe atom is in a $S = \frac{3}{2}$ spin configuration, as assumed in the quantum mechanical model.

To estimate the orbital moment and the MAE, we performed a relativistic calculation on a smaller three-layer-thick 4×4 slab of Cu(111) with a single Fe atom located in its lowest-energy relaxed position. Spin-orbit effects were accounted for using fully relativistic pseudopotentials acting on valence electron wave functions represented in the two-component spinor form [32]. The orbital moment was estimated by computing the expectation value of the orbital moment operator for the projection of the Khon-Sham wave functions on 3*d* orbitals of Fe. For the out-of-plane spin polarization, we find an orbital moment $\mu_L = 0.175$ μ_B and a spin moment $\mu_S = 3.16$ μ_B, in good agreement with our nonrelativistic result (3.24 μ_B). The low MAE obtained in our calculations was beyond the level of convergence we could achieve with respect to *k*-point sampling on a (3×3) mesh.

The reduced value for the calculated orbital moment compared with the experimental one is a well-known limitation of DFT calculations considering structural relaxation. On the contrary, calculations based on idealized bulklike distances minimize adatom-support hybridization thus giving larger orbital moment at the expense of an unrealistic geometry and electronic structure, as extensively discussed in Ref. [12]. For example, Lazarovits *et al.* [20] find $\mu_L = 0.65\mu_B$ and $K = 4.3$ meV, considering for the Fe atom a bulklike distance from the surface of 2.11 Å, about 10% larger than our value of 1.96 Å. To compare the spin magnetic moment obtained in DFT calculations with the one found with the sum rules we have to take into account only the polarization of the 3*d* orbitals, which are the ones probed by XAS and XMCD [33]. The DFT value, 3.09 μ_B both in the nonrelativistic model and in the relativistic one, is slightly higher than the experimental finding of $2.6 \pm 0.2\mu_B$. Overestimation of the spin moment in DFT calculations compared to sum rules values has been reported also for other systems [17]. The DFT value for the total spin is in good agreement with published DFT results, reported by Lazarovits *et al.*, $\mu_S = 3.27\mu_B$ [20], by Mavropoulos *et al.*, $3.24\mu_B$ [34], by Stepanyuk *et al.*, $3.17\mu_B$ [35], and by dos Santos Dias *et al.*, $3.23\mu_B$ [25].

B. Small Fe clusters on Cu(111)

The evolution of the spectral features and of the magnetic moments upon formation of small Fe clusters was investigated by increasing the Fe coverage up to $\Theta = 0.145$ ML at $T_{dep} \approx 3.5$ K. The XAS and XMCD spectra are shown in Fig. 5 with coverage increasing from top to bottom. The spectra evolve towards those of the bulk metal, with a gradual smoothening of the shoulders decorating the XAS and XMCD peaks, along with the disappearance of the small peak at the onset of the XMCD L_3 main peak. The disappearance of the low-energy component of the μ_- XAS L_3 peak results in a shift toward higher energies of the corresponding XMCD peak, up to a final value of 703.6 eV. Much in the same way, the evolution of the XAS L_2 double peak into a single feature results in an

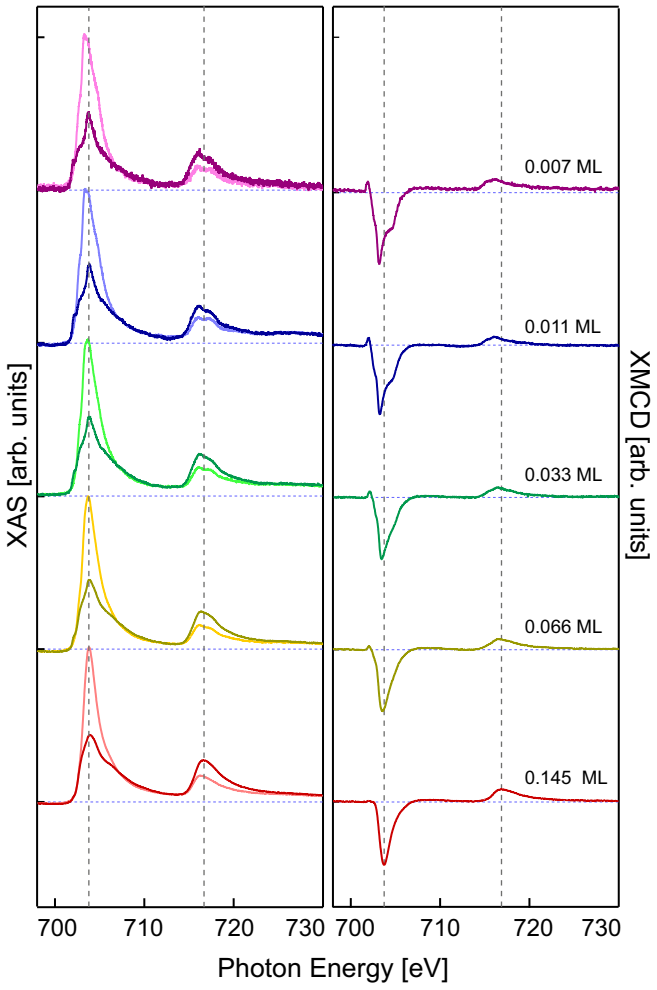

FIG. 5. (Color online) Background subtracted XAS (left) and XMCD (right) spectra at the Fe $L_{2,3}$ absorption edges for the indicated Fe coverages. Spectra were measured at $T = 2.5$ K, $B = 6.8$ T, and $\theta = 0°$. All XAS are normalized to one and vertically offset for clarity.

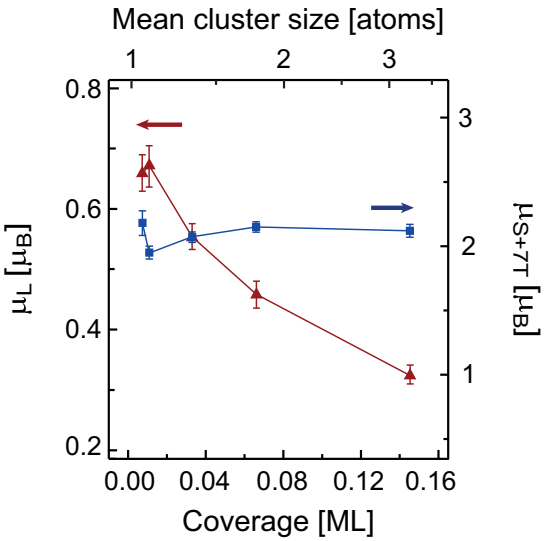

FIG. 6. (Color online) Orbital (triangles) and spin (squares) magnetic moments measured at normal incidence as a function of coverage (bottom) and mean cluster size (top). We assumed the single-atom value $h_d = 3.03$ given by multiplet calculations independently of cluster size.

upward shift of the corresponding XMCD resonance, that is located at 716.9 eV for the sample with the highest coverage. The smoothening of the multiplet structure with increasing coverage resembles the observations for Co atoms and clusters on K films [13] and on Pt(111) [1]. It is a consequence of the broadening of the adatom density of states due to d-state hybridization with the surrounding atoms in the cluster.

To correlate the observed spectral changes with the cluster sizes determining the signal at the respective coverages, we performed kinetic Monte Carlo (KMC) simulations [36]. The diffusion of Fe on Cu(111) was studied in the past. The diffusion barriers reported from DFT calculations are $E_m = 25$ [37], 22 [38], and 28 meV [39], and the barriers and attempt frequencies measured from temperature-dependent adatom diffusion rates are $E_m = 22 \pm 7$ meV, $\nu_0 = 1 \times 10^{10\pm2}$ Hz [39], and $E_m = 23.8 \pm 1.5$ meV, $\nu_0 = 4 \times 10^{8\pm1}$ Hz [40]. In our simulations, we take $E_m = 25$ meV and a universal preexponential factor of $\nu_0 = 10^{12}$ Hz. From this we find, in agreement with experiment, that the terrace diffusion of isolated Fe atoms is frozen at our $T_{dep} = 3.5$ K and that the diffusion rate is 30 Hz at 12 K, in agreement with the observation that Fe atoms organize at this temperature inside the voids of metal-organic honeycomb networks [41]. The formation of dimers has been reported to occur for Fe/Cu(111) by deposition of atoms close to other adatoms ($r \leqslant 0.6$ nm) and not by the lateral approach of adatoms that are further away [42]. In our simulations, we enable easy attachment of one Fe atom to a neighboring Fe atom or Fe cluster if it is two atomic distances apart [36]. The barrier for this process is chosen such that it always happens ($E_{att} = 0.1$ meV). The time intervening between the deposition and the end of measurements does not alter the size distributions since regular terrace diffusion does not take place, and all easy attachment processes have taken place immediately during deposition.

TABLE III. Coverage-dependent out-of-plane spin and orbital magnetic moments as obtained from the sum rules, $L_{2,3}$ branching ratios [$I(L_3)/I(L_2)$], and mean cluster size $\langle s \rangle$ calculated by KMC. The spin and orbital magnetic moments for 1 ML Fe on Cu(111) and for bulk Fe are also shown for comparison. We assumed $h_d = 3.03$, independent of cluster size, while $h_d = 3.4$ has been taken for the ML and bulk cases.

Coverage (ML)	μ_{S+7D} (μ_B)	μ_L (μ_B)	L_3/L_2	$\langle s \rangle$
0.007	2.2 ± 0.1	0.66 ± 0.04	4.2	1.07
0.011	1.95 ± 0.05	0.67 ± 0.05	4.4	1.12
0.033	2.07 ± 0.04	0.55 ± 0.03	4.3	1.37
0.066	2.15 ± 0.04	0.45 ± 0.03	3.9	1.82
0.145	2.12 ± 0.05	0.32 ± 0.02	3.3	3.25
1 [43]	0.7 ± 0.2	0.045 ± 0.015		
Bulk [17]	1.97	0.068	2.2	

Figure 6 shows the orbital and spin magnetic moments as function of coverage and the respective mean cluster size found in KMC. The corresponding values are given in Table III together with the branching ratios. Figure 7 shows for four Fe coverages the contributions of the different cluster sizes to the XAS intensity, i.e., the relative abundance of each size was multiplied by the number of atoms it contains.

In the spectra of Fig. 5, some multiplet-related features are observed for coverages up to 0.066 ML. By comparison with Fig. 7, we deduce that the multiplet structure disappears when the contribution of monomers to the overall XAS signal becomes negligible. We conclude that only monomers have a remainder of the atomiclike spectrum, while already dimers have a spectrum close to the bulk one. While the spin moment is size independent, the orbital moment rapidly decreases with increasing mean size, similar to the case of Co/Pt(111) [1]. The ratio of L_3 to L_2 x-ray absorption intensities (branching ratio) starts to decrease once the monomers are not the dominant species any more. The overall values are quite high considering that the statistical ratio of L_3:L_2 is 2:1, and crystal field and spin-orbit interaction normally cause a reduction. However, large branching ratios were observed for small Fe clusters

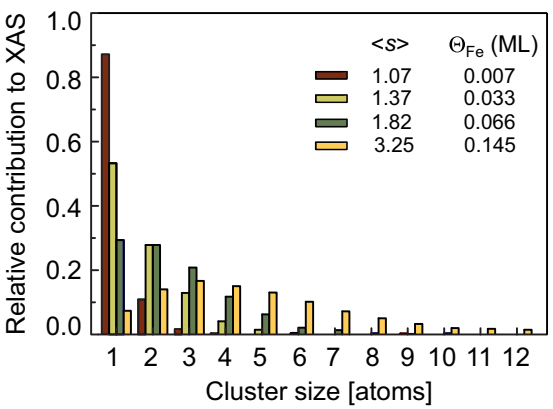

FIG. 7. (Color online) Cluster size distributions determined from KMC multiplied by the respective size in order to yield the contribution of each cluster size to the overall XAS intensity for the four displayed coverages.

in the gas phase and attributed to size-dependent core-hole screening [44,45].

We finally comment on the total magnetic moment of $15\mu_B$ assumed in Ref. [7] for an Fe_5 cluster on Cu(111). As shown in Fig. 6, the orbital moment rapidly decreases with increasing cluster size, and for a cluster of five atoms we estimate $\mu_L \approx 0.2\,\mu_B$ per atom. With $\mu_S \approx 2.4\mu_B$ per atom (the value of μ_{7T} rapidly decreases with cluster formation owing to the hybridization with the neighboring atoms, so we can assume it is small for a five-atom cluster) and an induced polarization on the copper atoms that can be neglected, as also this quantity decreases upon cluster formation, we find a total magnetic moment of $13\,\mu_B$, i.e., assuming $g = 2$ as in Ref. [7], a total angular moment of $\frac{13}{2}$. This slightly smaller value, however, does not affect the main conclusion of Ref. [7] that the half-integer value of the spin ground state forbids quantum tunneling, thus allowing for a long spin lifetime.

IV. CONCLUSIONS

We reported on the unexpected observation of XAS and XMCD multiplet features for Fe atoms on Cu(111), and on their gradual disappearing with increasing coverage and mean cluster size. We measured the spin, orbital, and total magnetic moments as well as the magnetic anisotropy energy for single Fe atoms adsorbed on Cu(111) and compared the obtained values with the ones predicted by DFT. The ground state of the Fe atoms on Cu(111) was found to be close to a $4s^1\ 3d^7$ configuration and the hybridization with the Cu substrate was shown to be low. We also demonstrated how the formation of small clusters influences the evolution of the orbital magnetic moment and of the branching ratio, while the spin magnetic moment is, at the small sizes considered and within our resolution, insensitive to cluster size.

ACKNOWLEDGMENTS

We acknowledge J. Dreiser and C. Piamonteze for their assistance with the experiments at X-Treme. We thank the Swiss National Science Foundation for financial support. G.A. and O.V.Y. acknowledge the Swiss National Science Foundation (Grant No. PP00P2_133552) and NCCR-MARVEL. First-principles calculations have been performed at the Swiss National Supercomputing Center (CSCS) under Project No. s515.

[1] P. Gambardella, S. Rusponi, M. Veronese, S. S. Dhesi, C. Grazioli, A. Dallmeyer, I. Cabria, R. Zeller, P. H. Dederichs, K. Kern, C. Carbone, and H. Brune, Giant magnetic anisotropy of single Co atoms and nanoparticles on Pt, Science **300**, 1130 (2003).

[2] F. Meier, L. Zhou, J. Wiebe, and R. Wiesendanger, Revealing magnetic interactions from single-atom magnetization curves, Science **320**, 82 (2008).

[3] H. Brune and P. Gambardella, Magnetism of individual atoms adsorbed on surfaces, Surf. Sci. **603**, 1812 (2009).

[4] I. G. Rau, S. Baumann, S. Rusponi, F. Donati, S. Stepanow, L. Gragnaniello, J. Dreiser, C. Piamonteze, F. Nolting, S. Gangopadhyay, O. R. Albertini, R. M. Macfarlane, C. P. Lutz, B. A. Jones, P. Gambardella, A. J. Heinrich, and H. Brune, Reaching the magnetic anisotropy limit of a 3d metal atom, Science **344**, 988 (2014).

[5] A. A. Khajetoorians, J. Wiebe, B. Chilian, and R. Wiesendanger, Realizing all-spin-based logic operations atom by atom, Science **332**, 1062 (2011).

[6] A. A. Khajetoorians, J. Wiebe, B. Chilian, S. Lounis, S. Blügel, and R. Wiesendanger, Atom-by-atom engineering and magnetometry of tailored nanomagnets, Nat. Phys. **8**, 497 (2012).

[7] A. A. Khajetoorians, B. Baxevanis, C. Hübner, T. Schlenk, S. Krause, T. O. Wehling, S. Lounis, A. Lichtenstein, D. Pfannkuche, J. Wiebe, and R. Wiesendanger, Current-driven spin dynamics of artificially constructed quantum magnets, Science **339**, 55 (2013).

[8] A. A. Khajetoorians, S. Lounis, B. Chilian, A. T. Costa, L. Zhou, D. L. Mills, J. Wiebe, and R. Wiesendanger, Itinerant nature of atom-magnetization excitation by tunneling electrons, Phys. Rev. Lett. **106**, 037205 (2011).

[9] C. Carbone, M. Veronese, P. Moras, S. Gardonio, C. Grazioli, P. H. Zhou, O. Rader, A. Varykhalov, C. Krull, T. Balashov, A. Mugarza, P. Gambardella, S. Lebègue, O. Eriksson, M. I. Katsnelson, and A. I. Lichtenstein, Correlated electrons step by step: Itinerant-to-localized transition of Fe impurities in free-electron metal hosts, Phys. Rev. Lett. **104**, 117601 (2010).

[10] A. Lehnert, Magnetism of individual adatoms and of epitaxial monolayers, Ph.D. thesis, EPFL, 2009.

[11] A. A. Khajetoorians, T. Schlenk, B. Schweflinghaus, M. dos Santos Dias, M. Steinbrecher, M. Bouhassoune, S. Lounis, J. Wiebe, and R. Wiesendanger, Spin excitations of individual Fe atoms on Pt(111): Impact of the site-dependent giant substrate polarization, Phys. Rev. Lett. **111**, 157204 (2013).

[12] P. Błoński, A. Lehnert, S. Dennler, S. Rusponi, M. Etzkorn, G. Moulas, P. Bencok, P. Gambardella, H. Brune, and J. Hafner, Magnetocrystalline anisotropy energy of Co and Fe adatoms on the (111) surfaces of Pd and Rh, Phys. Rev. B **81**, 104426 (2010).

[13] P. Gambardella, S. S. Dhesi, S. Gardonio, C. Grazioli, P. Ohresser, and C. Carbone, Localized magnetic states of Fe, Co, and Ni impurities on alkali metal films, Phys. Rev. Lett. **88**, 047202 (2002).

[14] B. T. Thole, P. Carra, F. Sette, and G. van der Laan, X-ray circular dichroism as a probe of orbital magnetization, Phys. Rev. Lett. **68**, 1943 (1992).

[15] P. Carra, B. T. Thole, M. Altarelli, and X. Wang, X-ray circular dichroism and local magnetic fields, Phys. Rev. Lett. **70**, 694 (1993).

[16] C. Piamonteze, U. Flechsig, S. Rusponi, J. Dreiser, J. Heidler, M. Schmidt, R. Wetter, M. Calvi, T. Schmidt, H. Pruchova, J. Krempasky, C. Quitmann, H. Brune, and F. Nolting, X-Treme beamline at SLS: X-ray magnetic circular and linear dichroism at high field and low temperature, J. Synchrotron Radiat. **19**, 661 (2012).

[17] C. T. Chen, Y. U. Idzerda, H.-J. Lin, N. V. Smith, G. Meigs, E. Chaban, G. H. Ho, E. Pellegrin, and F. Sette, Experimental confirmation of the X-ray magnetic circular dichroism sum rules for iron and cobalt, Phys. Rev. Lett. **75**, 152 (1995).

[18] A. Lehnert, S. Rusponi, M. Etzkorn, S. Ouazi, P. Thakur, and H. Brune, Magnetic properties of Fe and Co adatoms and Fe clusters magnetically decoupled from Ni_3 Al(111) by an alumina bilayer, Phys. Rev. B **81**, 104430 (2010).

[19] P. Gambardella, S. Stepanow, A. Dmitriev, J. Honolka, F. M. F. de Groot, M. Lingerfelder, S. Sen Gupta, D. D. Sarma, Bencok P., S. Stanescu, S. Clair, S. Pons, N. Lin, A. P. Seitsonen, H. Brune, J. V. Barth, and K. Kern, Supramolecular control of the magnetic anisotropy in two-dimensional high-spin Fe arrays at a metal interface, Nat. Mater. **8**, 189 (2009).

[20] B. Lazarovits, L. Szunyogh, P. Weinberger, and B. Újfalussy, Magnetic properties of finite Fe chains at fcc Cu(001) and Cu(111) surfaces, Phys. Rev. B **68**, 024433 (2003).

[21] E. Stavitski and F. M. F. de Groot, The CTM4XAS program for EELS and XAS spectral shape analysis of transition metal *L* edges, Micron **41**, 687 (2010).

[22] D. Weller, J. Stöhr, R. Nakajima, A. Carl, M. G. Samant, C. Chappert, R. Mégy, P. Beauvillain, P. Veillet, and G. A. Held, Microscopic origin of magnetic anisotropy in Au/Co/Au probed with X-ray magnetic circular dichroism, Phys. Rev. Lett. **75**, 3752 (1995).

[23] C. Piamonteze, P. Miedema, and F. M. F. de Groot, Accuracy of the spin sum rule in XMCD for the transition-metal *L* edges from manganese to copper, Phys. Rev. B **80**, 184410 (2009).

[24] F. Donati, L. Gragnaniello, A. Cavallin, F. D. Natterer, Q. Dubout, M. Pivetta, F. Patthey, J. Dreiser, C. Piamonteze, S. Rusponi, and H. Brune, Tailoring the magnetism of Co atoms on graphene through substrate hybridization, Phys. Rev. Lett. **113**, 177201 (2014).

[25] M. dos Santos Dias, B. Schweflinghaus, S. Blügel, and S. Lounis, Relativistic dynamical spin excitations of magnetic adatoms, Phys. Rev. B **91**, 075405 (2015).

[26] B. Chilian, A. A. Khajetoorians, S. Lounis, A. T. Costa, D. L. Mills, J. Wiebe, and R. Wiesendanger, Anomalously large *g* factor of single atoms adsorbed on a metal substrate, Phys. Rev. B **84**, 212401 (2011).

[27] V. I. Anisimov, J. Zaanen, and O. K. Andersen, Band theory and Mott insulators: Hubbard U instead of Stoner I, Phys. Rev. B **44**, 943 (1991).

[28] P. Giannozzi *et al.*, QUANTUM ESPRESSO: a modular and open-source software project for quantum simulations of materials, J. Phys.: Condens. Matter **21**, 395502 (2009).

[29] M. Cococcioni and S. de Gironcoli, Linear response approach to the calculation of the effective interaction parameters in the LDA+U method, Phys. Rev. B **71**, 035105 (2005).

[30] M. Emmrich, F. Huber, F. Pielmeier, J. Welker, T. Hofmann, M. Schneiderbauer, D. Meuer, S. Polesya, S. Mankovsky, D. Ködderitzsch, H. Ebert, and F. J. Giessibl, Subatomic resolution force microscopy reveals internal structure and adsorption sites of small iron clusters, Science **348**, 308 (2015).

[31] J. Repp, G. Meyer, K.-H. Rieder, and P. Hyldgaard, Site determination and thermally assisted tunneling in homogenous nucleation, Phys. Rev. Lett. **91**, 206102 (2003).

[32] A. Dal Corso and A. Mosca Conte, Spin-orbit coupling with ultrasoft pseudopotentials: Application to Au and Pt, Phys. Rev. B **71**, 115106 (2005).

[33] H. Ebert, J. Stöhr, S. S. P. Parkin, M. Samant, and A. Nilsson, *L* -edge x-ray absorption in fcc and bcc Cu metal: Comparison of experimental and first-principles theoretical results, Phys. Rev. B **53**, 16067 (1996).

[34] P. Mavropoulos, S. Lounis, R. Zeller, and S. Blügel, Fe clusters on Ni and Cu: size and shape dependence of the spin moment, Appl. Phys. A **82**, 103 (2006).

[35] V. S. Stepanyuk, L. Niebergall, R. C. Longo, W. Hergert, and P. Bruno, Magnetic nanostructures stabilized by surface-state electrons, Phys. Rev. B **70**, 075414 (2004).

[36] H. Brune, Microscopic view of epitaxial metal growth: nucleation and aggregation, Surf. Sci. Rep. **31**, 125 (1998).

[37] Y. Mo, K. Varga, E. Kaxiras, and Z. Zhang, Kinetic pathway for the formation of Fe nanowires on stepped Cu(111) surfaces, Phys. Rev. Lett. **94**, 155503 (2005).

[38] N. N. Negulyaev, V. S. Stepanyuk, W. Hergert, P. Bruno, and J. Kirschner, Atomic-scale self-organization of Fe nanostripes on stepped Cu(111) surfaces: Molecular dynamics and kinetic Monte Carlo simulations, Phys. Rev. B **77**, 085430 (2008).

[39] N. N. Negulyaev, V. S. Stepanyuk, L. Niebergall, P. Bruno, W. Auwärter, Y. Pennec, G. Jahnz, and J. V. Barth, Effect of strain relaxations on heteroepitaxial metal-on-metal island nucleation and superlattice formation: Fe on Cu(111), Phys. Rev. B **79**, 195411 (2009).

[40] X. P. Zhang, B. F. Miao, L. Sun, C. L. Gao, An Hu, H. F. Ding, and J. Kirschner, Atomic superlattice formation mechanism revealed by scanning tunneling microscopy and kinetic Monte Carlo simulations, Phys. Rev. B **81**, 125438 (2010).

[41] M. Pivetta, G. E. Pacchioni, U. Schlickum, J. V. Barth, and H. Brune, Formation of Fe cluster superlattice in a metal-organic quantum-box network, Phys. Rev. Lett. **110**, 086102 (2013).

[42] J. Hu, B. Teng, F. Wu, and Y. Fang, Fe nanostructures stabilized by long-range interactions on Cu(111): kinetic Monte Carlo simulations, New J. Phys. **10**, 023033 (2008).

[43] P. Ohresser, G. Ghiringhelli, O. Tjernberg, N. B. Brookes, and M. Finazzi, Magnetism of nanostructures studied by X-ray magnetic circular dichroism: Fe on Cu(111), Phys. Rev. B **62**, 5803 (2000).

[44] J. T. Lau, J. Rittmann, V. Zamudio-Bayer, M. Vogel, K. Hirsch, Ph. Klar, F. Lofink, T. Möller, and B. v. Issendorff, Size-dependence of $L_{2,3}$ branching ratio and $2p$ core-hole screening in X-ray absorption of metal clusters, Phys. Rev. Lett. **101**, 153401 (2008).

[45] K. Hirsch, V. Zamudio-Bayer, J. Rittmann, A. Langenberg, M. Vogel, T. Möller, B. v. Issendorff, and J. T. Lau, Initial- and final-state effects on screening and branching ratio in $2p$ X-ray absorption of size-selected free $3d$ transition metal clusters, Phys. Rev. B **86**, 165402 (2012).